

Supporting information

Regulating orientation of coordinate bonds by synergistic action of mechanical forces and electric field

Wei Zhang¹, Zhibin Zhao¹, Min Tan¹, Adila Adijiang¹, Shurong Zhong¹, Xiaona Xu¹, Tianran Zhao¹, Emusani Ramya¹, Lu Sun¹, Xueyang Zhao¹, Zhiqiang Fan^{2,}, Dong Xiang^{1,3*}*

¹Institute of Modern Optics and Center of Single Molecule Sciences, Nankai University, Key Laboratory of Micro-scale Optical Information Science and Technology, Tianjin 300350, China.

²School of Physics and Electronic Science, Changsha University of Science and Technology, Changsha 410114, China.

³School of Materials Science and Engineering, Smart Sensing Interdisciplinary Science Center, Nankai University, Tianjin 300350, China.

Table of contents

1. Fabrication of STM tip and substrate
2. Conductance of single-molecule break junctions under different bias
3. I-V measurement of fixed molecular junctions
4. Flicker noise power spectroscopy
5. DFT calculation of electron transport through molecular junctions
6. Molecular electrostatic potential distribution
7. Reference

1. Fabrication of STM tip and substrate

STM tips are prepared by burning one end of the clean gold wire ($d = 0.25$ mm) with an n-butane flame to form pellets, as shown in Figure S1a. The bottom gold substrates are fabricated as follows. Firstly, the $1.0\text{ cm} \times 2.0\text{ cm}$ silicon wafers are immersed in acetone/ethanol solution and ultrasonically cleaned for more than 20 minutes. Secondly, the cleaned silicon wafers are dried with nitrogen, and coated with 10 nm chromium (Cr) layer and 200 nm gold film by magnetron-controlled ion sputtering machine (ISC150 PRO, China; 20 W and 10 s for sputtering Cr; 12 W and 260 s for sputtering Au). A schematic diagram of the cross-section of the substrate is shown in Figure S1b, and the top view of the substrate is shown in Figure S1c.

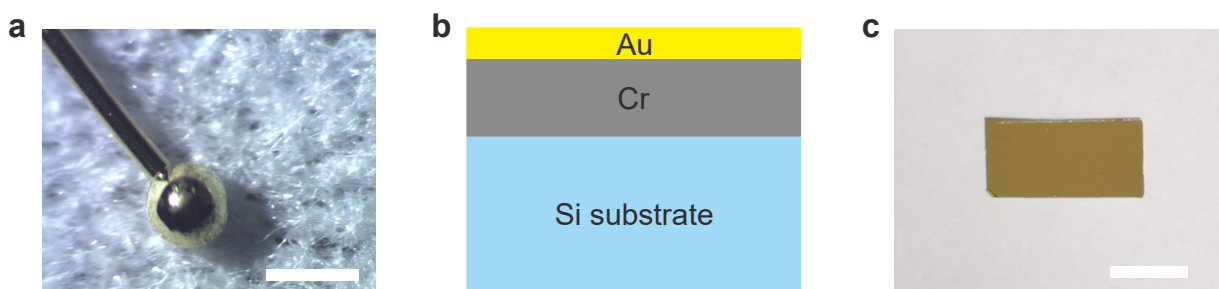


Figure S1. Fabrication of top and bottom gold electrodes. (a) Optical image of the Au tip on a paper. Scale bare: 1 mm. (b) Schematic diagram of the bottom Au substrate on top of the silicon wafer. (c) Optical image of the bottom substrate. Scale bar: 10 mm.

All molecules were purchased from Bidepharm and used without further purification. The target molecules (PY[4], PY[3], PY[2], NH₂[4], NH₂[3], NH₂[2]) were dissolved in 1,2,4-trichlorobenzene (Aladdin, > 99%) to prepare a molecular solution with a concentration of 0.5 mmol/L for electrical characterization. To make self-assembled molecules on the gold substrate, the bare gold substrate was immersed in the solution for 24 hours. The atomic force microscope (AFM) images of the bare gold substrate, self-assembling of PY[4], and self-assembling NH₂[4] were shown in Figure S2. AFM images were acquired from a Dimension Icon (Bruker) microscope operating in peak-force trapping mode, and the NanoScope Analysis software package (version 1.8) was used to analyze the acquired data. It can be found that the surface become smooth after self-assembling of PY[4]. In contrast, for NH₂[4] SAM, some bright spots can be observed due to the aggregation of NH₂[4] molecules under ambient conditions by forming the hydrogen bonds.

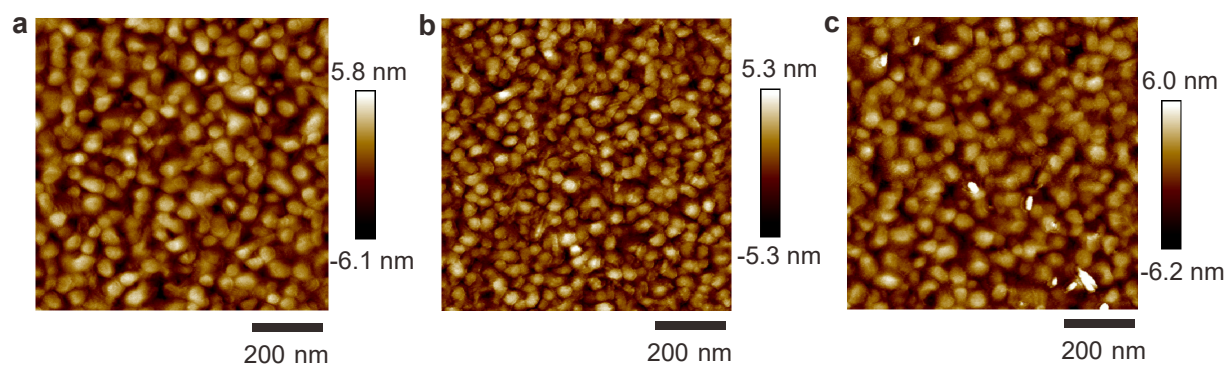


Figure S2. Three types of AFM images. (a) AFM image of gold-covered silicon substrate. The root mean square roughness and average roughness are 1.76 nm and 1.43 nm. (b) AFM image of PY[4] SAM on gold substrate. The root mean square roughness and average roughness are 1.58 nm and 1.28 nm. (c) AFM image of NH₂[4] SAM on gold substrate. The root mean square roughness and average roughness are 1.83 nm and 1.44 nm. Scan ranges: 1 μm \times 1 μm .

2. Conductance of single-molecule break junctions under different bias voltage

Two types of electrical measurements were performed after the target molecules-containing solution was dropped on the gold substrate. One is to use the STM-BJ approach to quantify the statistical conductance based on the dynamic molecular break junctions. A molecular junction can be repeatedly formed and broken by manipulating the displacement of the STM tip, in which the current flowing through the junctions varies as a function of the displacement of the tip electrode. The probable conductance of the junctions was determined by creating the conductance histograms using thousands of conductance-displacement traces. The alternative measurement is an I-V measurement that relies on fixed molecular junctions. In this measurement, the tip electrode is suspended as soon as a molecule junction forms, and as a result, the distance between the top tip electrode and bottom substrate electrode is fixed as well. A swept bias voltage is applied on the fixed molecule junction. To plot the I-V density image, approximately 3000 current-voltage curves were recorded.

Figures S3-S8 show the conductance histograms of two series molecular junctions at different positive and negative bias voltages. For pyridyl-anchored molecular junctions, the peak in one-dimensional (1D) conductance histograms left-shifts as higher bias voltages are applied. In contrast, for amino-anchored molecular junctions, the peak remains unchanged upon a higher bias. Meanwhile, it can be noted that, only for pyridyl-anchored molecular junctions, the plateaus length clearly decreases as higher bias voltages are applied, indicating a shorter life-time of the junctions (and a weaker coupling of the molecular junction) upon a higher bias.

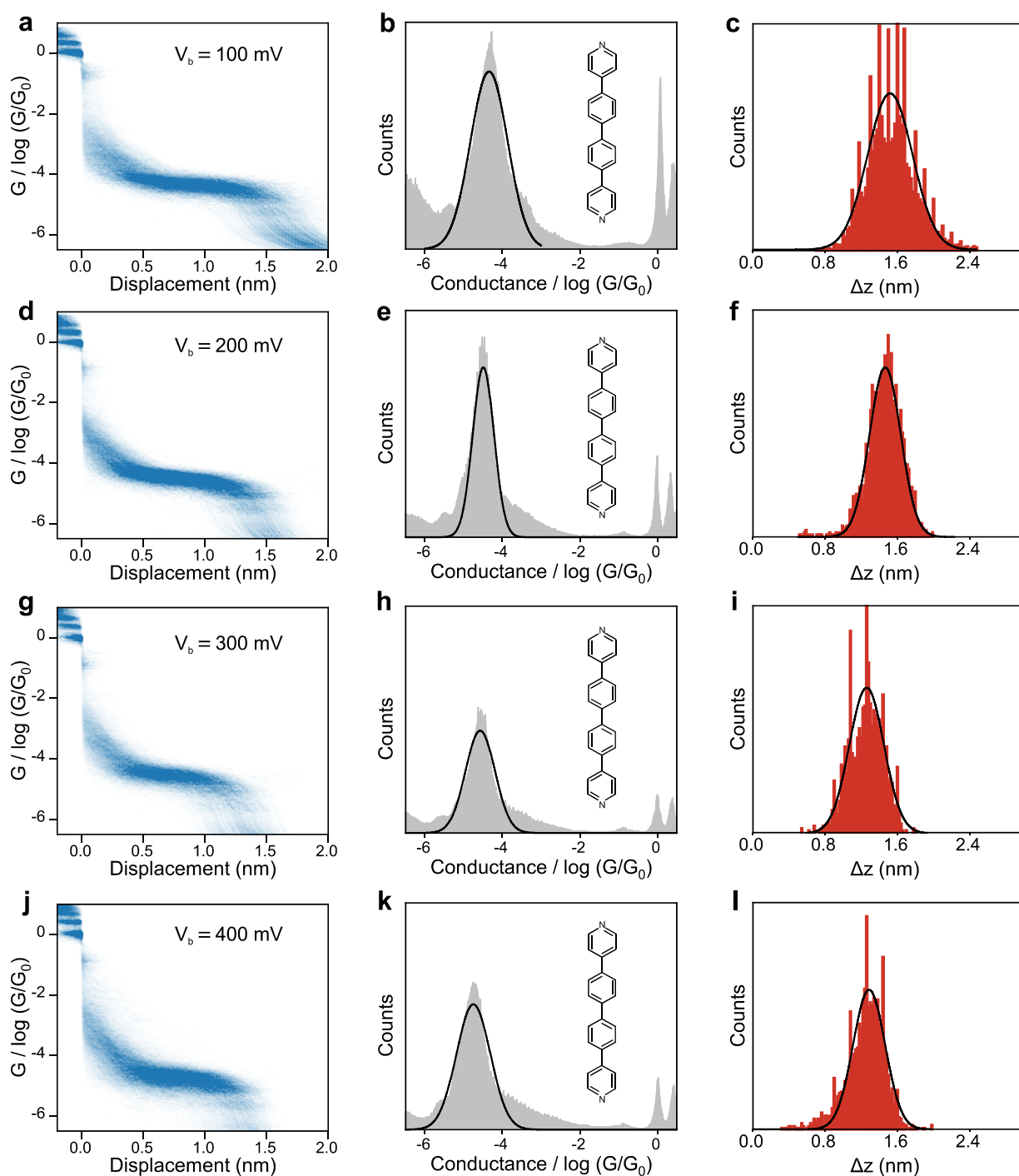


Figure S3. Single-molecule conductance of PY[4] molecular junctions at positive bias voltages. Particularly, 2D conductance-distance histograms, 1D conductance histograms, and corresponding conductance plateau length distributions of PY[4] molecular junctions under (a-c) 100 mV, (d-f) 200 mV, (g-i) 300 mV, (j-l) 400 mV, respectively.

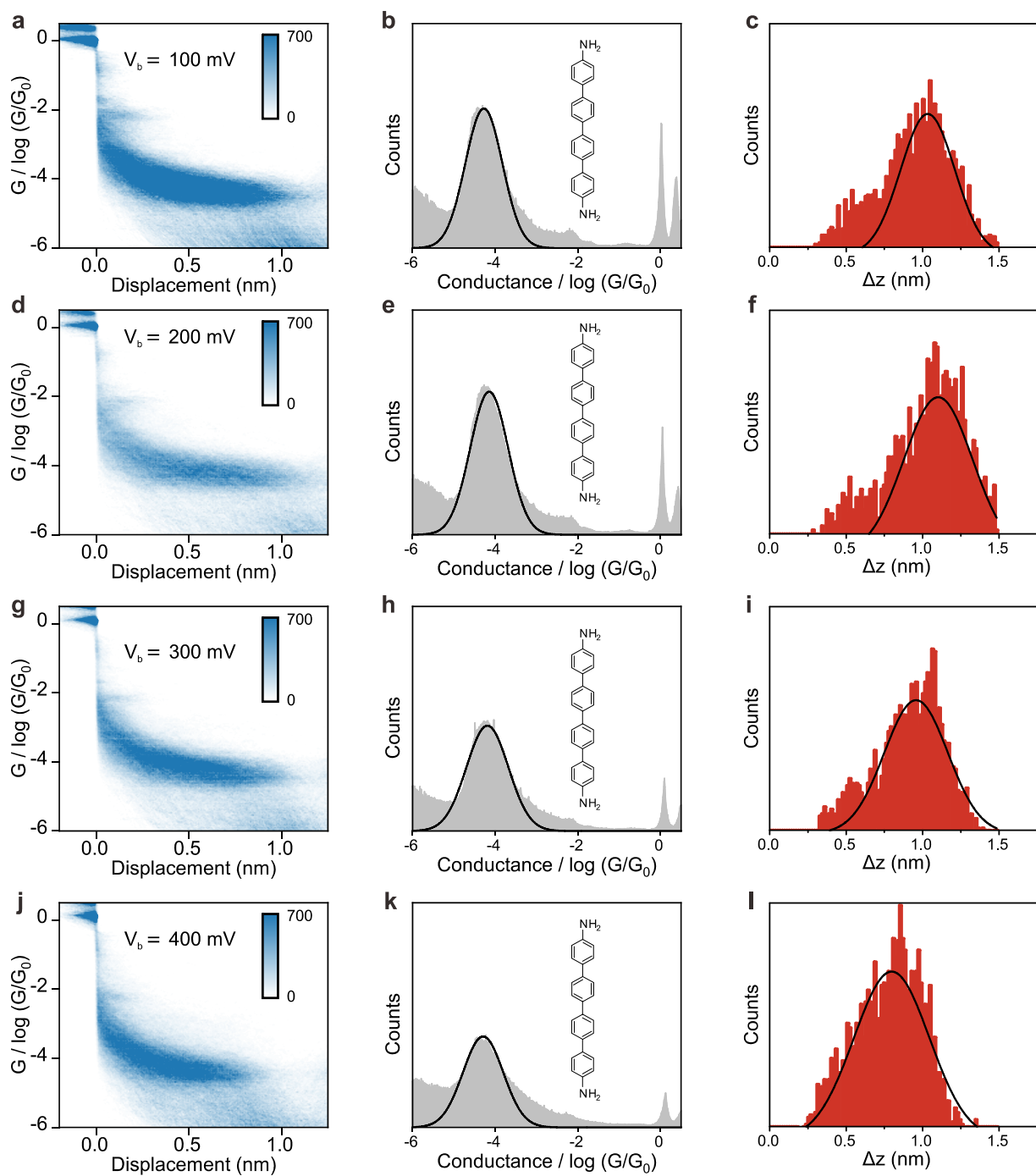


Figure S4. Conductance of NH₂[4] molecular junctions at positive bias voltages. Particularly, 2D conductance-distance histograms, 1D conductance histograms, and corresponding conductance plateau length distributions of NH₂[4] molecular junctions under (a-c) 100 mV, (d-f) 200 mV, (g-i) 300 mV, (j-l) 400 mV, respectively.

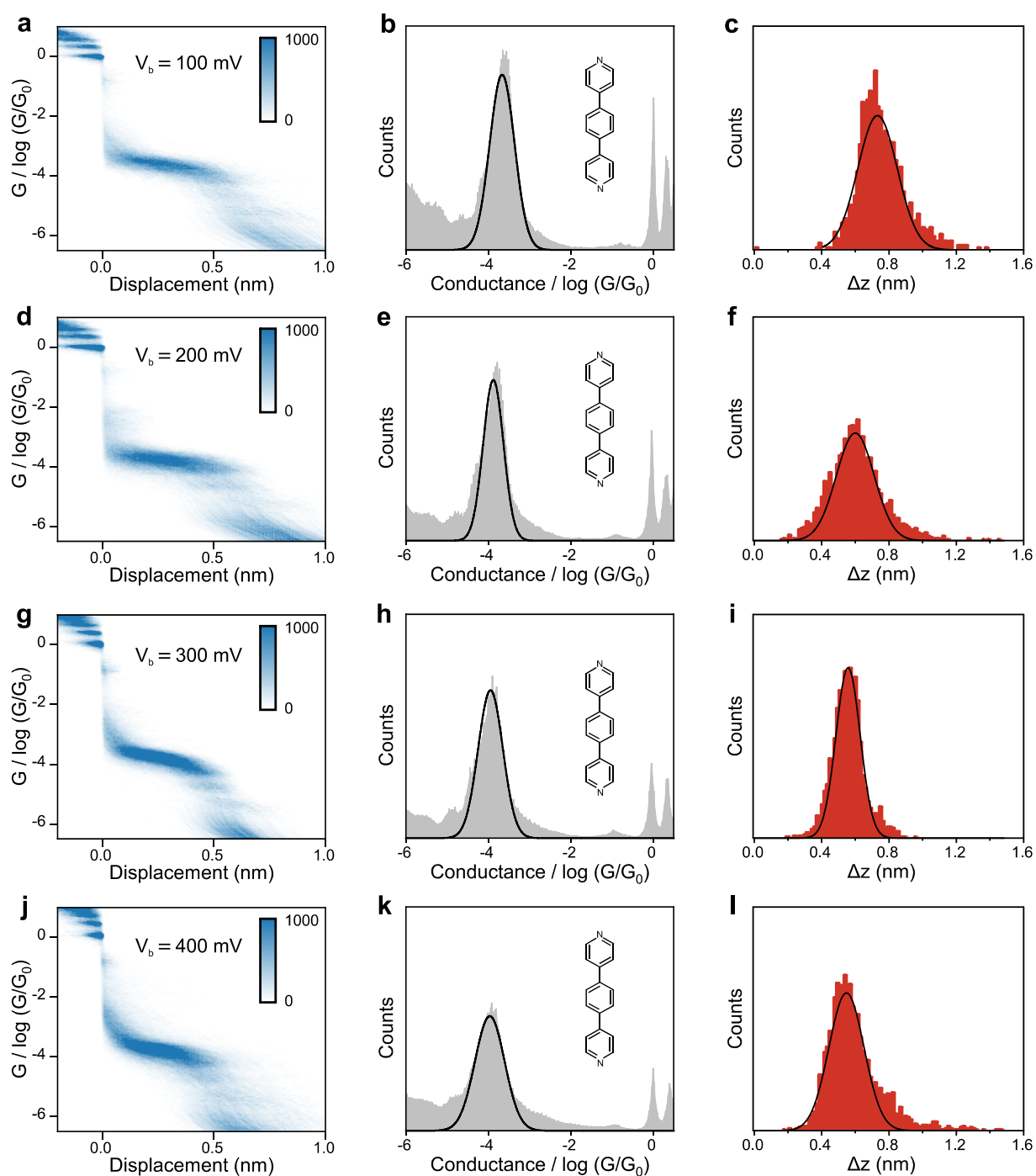


Figure S5. Single-molecule conductance of PY[3] molecular junctions at positive bias voltages. Particularly, 2D conductance-distance histograms, 1D conductance histograms, and corresponding conductance plateau length distributions of PY[3] molecular junctions under (a-c)100 mV, (d-f) 200 mV, (g-i) 300 mV, (j-l) 400 mV, respectively.

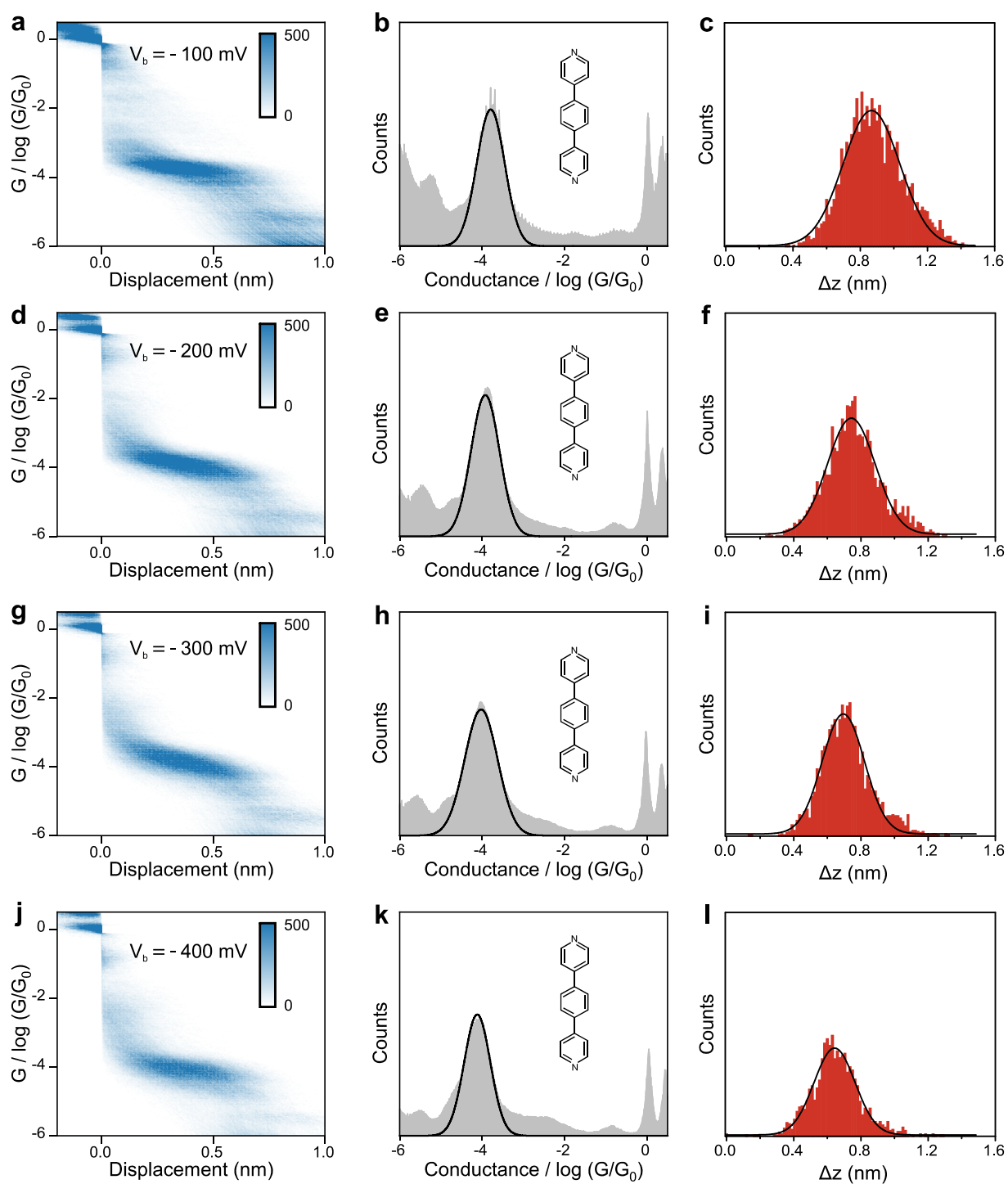


Figure S6. Single-molecule conductance of PY[3] molecular junctions at negative bias voltages. 2D (1D) conductance histograms and conductance plateau length distributions of PY[3] junctions under (a-c) -100 mV, (d-f) -200 mV, (g-i) -300 mV, (j-l) -400 mV, respectively.

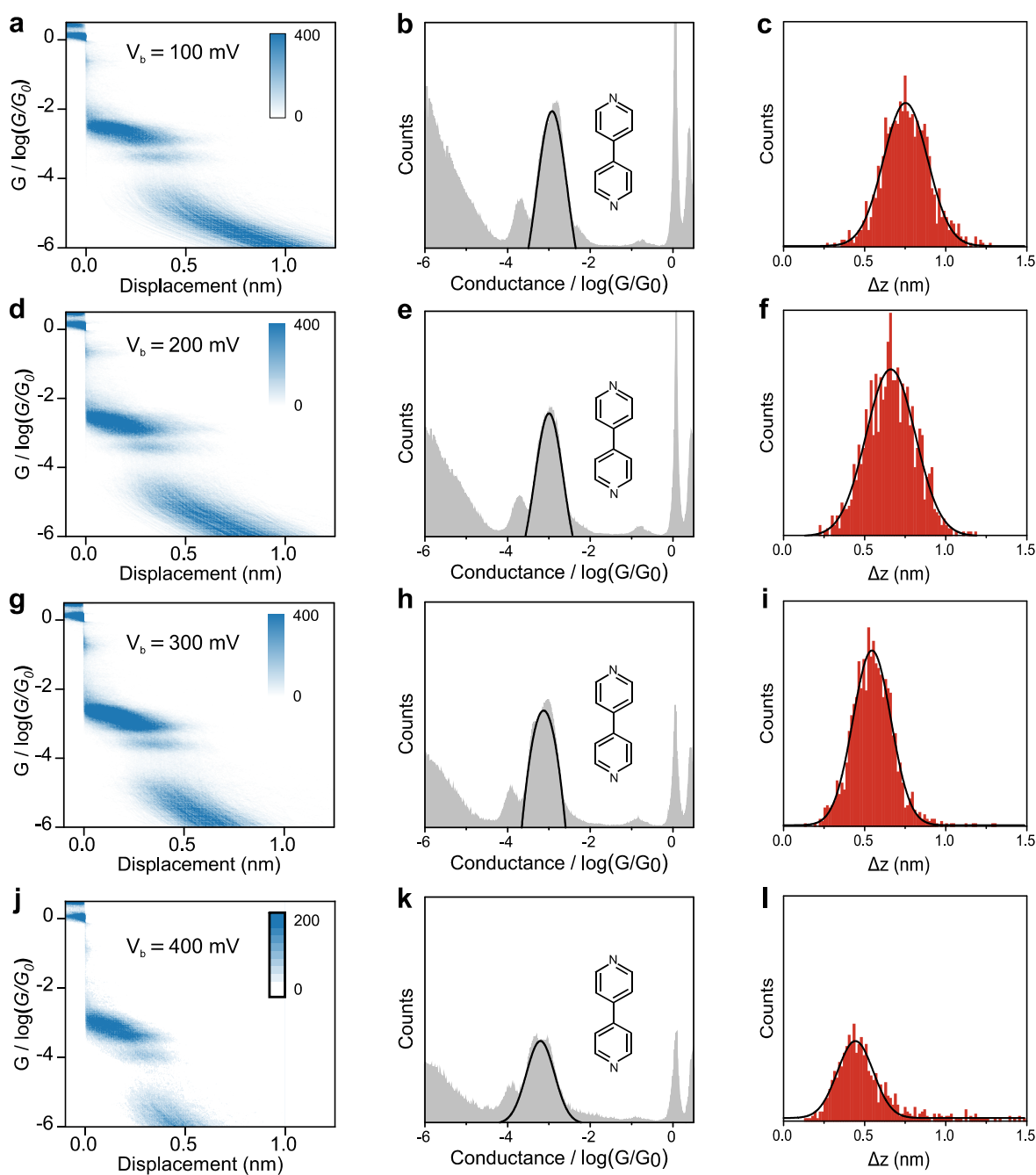


Figure S7. Single-molecule conductance of PY[2] molecular junctions at positive bias voltages. Particularly, 2D conductance-distance histograms, 1D conductance histograms, and corresponding conductance plateau length distributions of PY[2] molecular junctions under (a-c) 100 mV, (d-f) 200 mV, (g-i) 300 mV, (j-l) 400 mV, respectively.

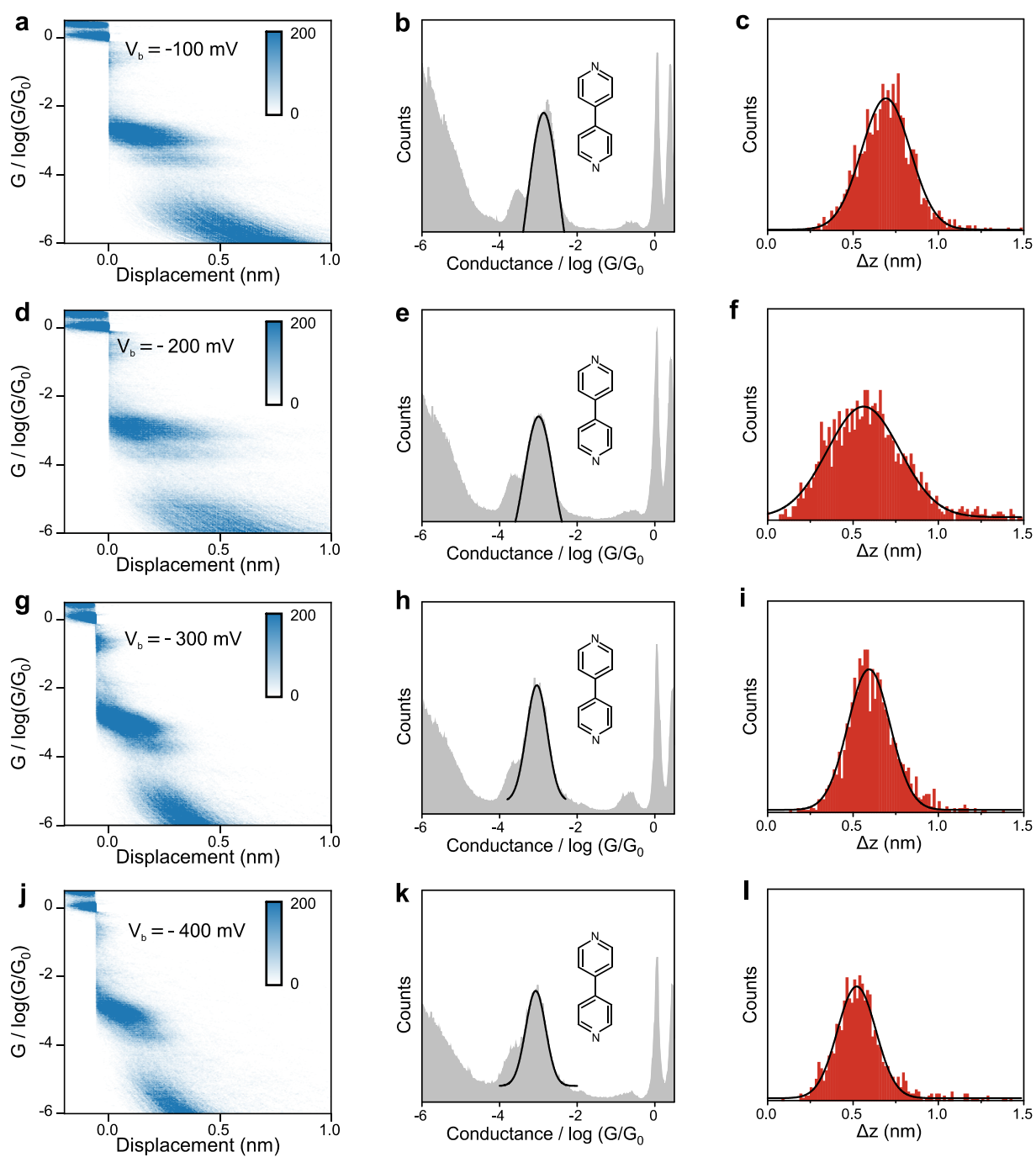
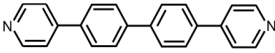
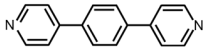
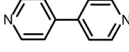
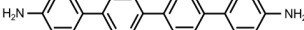

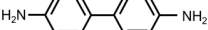


Figure S8. Single-molecule conductance of PY[2] molecular junctions at negative bias voltages. 2D conductance-distance histograms, 1D conductance histograms, and corresponding conductance plateau length distributions of PY[2] molecular junctions under (a-c) -100 mV, (d-f) -200 mV, (g-i) -300 mV, (j-l) -400 mV, respectively.

Table S1 summarizes the chemical structures of the molecules and the correspondingly probable conductances of the molecular junctions at negative bias voltages, determined by Gaussian fitting of the peak of conductance histograms. In case of that there are multiple peaks in the conductance histogram, only the high conductance (main peak) is listed in this table. It can be found that the conductance variation for long molecule is larger than the one for short molecule as the bias voltage increases. We attribute it to the factors that the molecular junctions with longer molecular length will be exposed to electric field and mechanical stretching with longer duration time before its breakage. As a result, the orientation of nitrogen-gold bonds has higher probability to be modulated to align with the electric field. The orientation change of the nitrogen-gold bonds will lead to the conductance change. Therefore, PY[4] shows larger conductance variation compared to PY[2] as the bias voltage increases.

Table S1. The structures of the molecules and corresponding probable conductance determined by Gaussian fitting the peak of 1D conductance histograms under negative biases.

Molecule	Structure	Conductance (G_0)			
		@-100 mV	@-200 mV	@-300 mV	@-400 mV
PY [4]		3.7×10^{-5}	1.99×10^{-5}	1.77×10^{-5}	8.56×10^{-6}
PY [3]		1.5×10^{-4}	1.36×10^{-4}	9.68×10^{-5}	7.21×10^{-5}
PY [2]		1.36×10^{-3}	1.01×10^{-3}	9.11×10^{-4}	8.51×10^{-4}
NH ₂ [4]		3.7×10^{-5}	3.67×10^{-5}	3.57×10^{-5}	3.77×10^{-5}
NH ₂ [3]		1.82×10^{-4}	1.69×10^{-4}	1.71×10^{-4}	1.88×10^{-4}
NH ₂ [2]		8.55×10^{-4}	8.37×10^{-4}	7.94×10^{-4}	5.89×10^{-4}

With a close examination, it can be found that there are significant discrepancies between negative and positive voltage results for pyridyl based junctions, as shown in Table 1 and Table S1. It can be attributed to the asymmetric geometry of the electrodes prepared different methods. The top electrode is prepared by burning one end of the microscale gold wire but the bottom electrode is fabricated by sputtering gold wire on silicon wafer. Therefore, the top and bottom electrode may possess different geometry during the repeated contact and break process. The different electrode geometry will lead to the different contact interfaces at two terminals, *e.g.*, the flat electrode tends to form π -coupling with pyridine-anchored molecule, while it is relatively difficult for the electrode with sharp-tip geometry¹. The asymmetric molecular junctions will show different conductance under polar bias voltages.

Figure S9a shows the 1D conductance histograms of p-Terphenyl-4,4''-dithiol (labeled as SH[3]) molecular junctions at different bias voltages. SH[3] have the same backbone as PY[3] and NH₂[3] but different anchoring group, *i.e.*, the SH[3] bond to the electrode *via* thiol anchoring group rather than pyridine (amino) anchoring group, as shown in Figure S9b. 2D conductance histogram under different bias are shown in Figure S9c-9f. It can be found that the probable conductance of SH[3] molecular junctions remains almost constant and is independent on bias voltage.

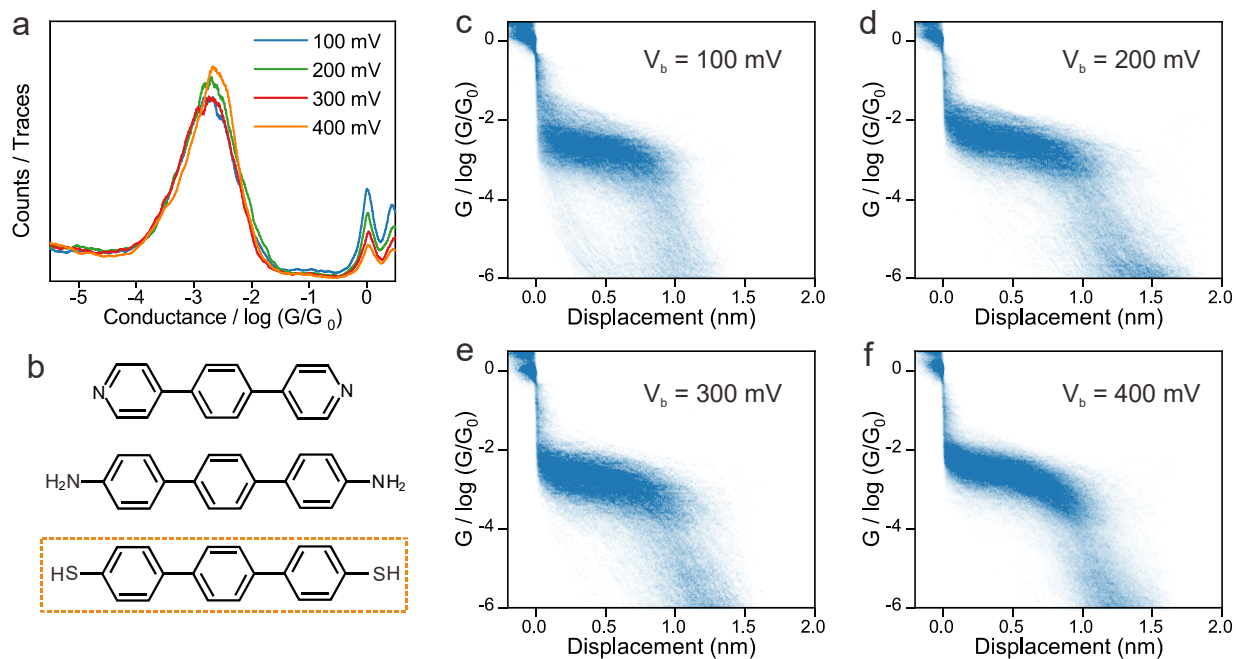


Figure S9. (a) 1D conductance histograms for SH[3] molecular junctions at bias voltages of 100 mV (blue), 200 mV (green), 300 mV (red), and 400 mV (orange). (b) Molecular structures of PY[3] (top), NH₂[3] (middle), and SH[3] (bottom) molecules. (c-f) 2D conductance-distance histograms of SH[3] molecular junctions at different bias voltages.

3. I-V measurement of fixed molecular junctions

The I-V curves of the single-molecule junctions are obtained as follows. Initially, the STM tip is in contact with the bottom substrate (molecular junction formation) and then retract from the substrate (single molecular junction break) at a speed of 30 nm/s under a fixed bias of 100 mV. Upon molecular junction formation, as monitored by the current, the tip movement pauses, and the tip position is held for 150 ms. During the hold period, as shown in Figure S9a, the bias voltage first sweeps from 0 V to 1.5 V in 25 ms and maintained at 1.5 V for 25 ms. Then, the voltage sweeps from 1 V to -1.5 V in 50 ms and held at -1.5 V for 25 ms. Finally, the voltage sweeps from -1 V to 0 V to complete a sweep circle, as shown in Figure S10a. After one voltage sweep circle, the bias voltage was reset to a constant value (100 mV), and the state of the junction was reassessed. Only for those junctions that survived in the voltage sweeping process, the corresponding I-V curves were saved, and only the I-V curve recorded during the sweep process from 1.5 V to -1.5 V is used for the density plotting of I-V and G-V, as shown in Figure S10b. This I-V measurement process is repeated more than 3,000 times, then a contour plot of I-V and G-V can be obtained, as presented in Figure 3 in the main text.

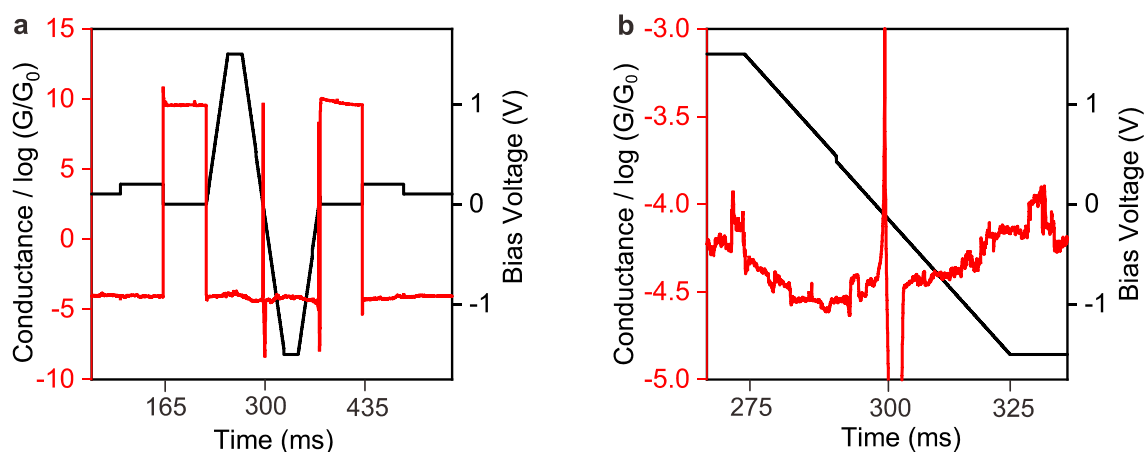


Figure S10. Real-time I-V measurements of single molecular junctions. (a) The actual process of the I-V scan. The black line shows the applied biased voltage on the molecular junction, and the red line shows the measured conductance of the molecular junction. (b) Zoomed area of a.

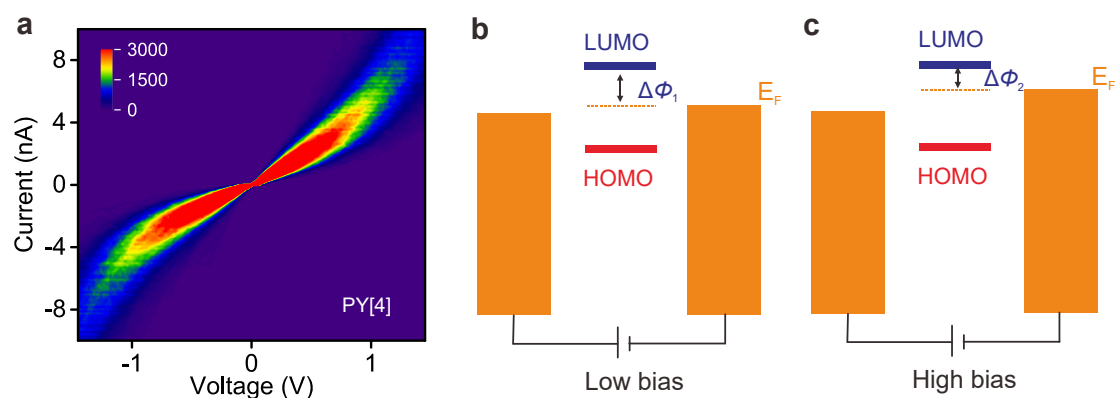


Figure S11. Typical I-V curves and energy landscape of the molecule junction under different bias voltage. (a) Density plots of I-V curves for PY[4] molecular junction. (b) Energy structure of the molecular junction at low bias. $\Delta\Phi_1$ denotes the energy gap between LUMO and E_F under low bias voltage. (c) Energy structure of the molecular junction at high bias. $\Delta\Phi_2 < \Delta\Phi_1$, which indicates that the energy barrier for electron transport at high bias is smaller than the one at low bias voltage, resulting an S-shape I-V curves during the voltage sweeping process, *i.e.*, the conductance of the molecular junction increase as the voltage increases.

4. Flicker noise power spectroscopy

To measure the flicker noise, the junction elongation procedure is halted for 150 ms at the position where the detected conductance is close to the probable conductance value determined by the conductance histogram (a stable molecular junction formation). The conductance is recorded at applied bias of 100 mV using a sampling rate of 20 kHz. The traces with a conductance within two standard deviations of the molecular conductance window at the beginning and the end of this hold-on period are extracted for discrete Fourier transform. Meanwhile, the average conductance (G_{AVG}) of this junction during the hold-on period is calculated.

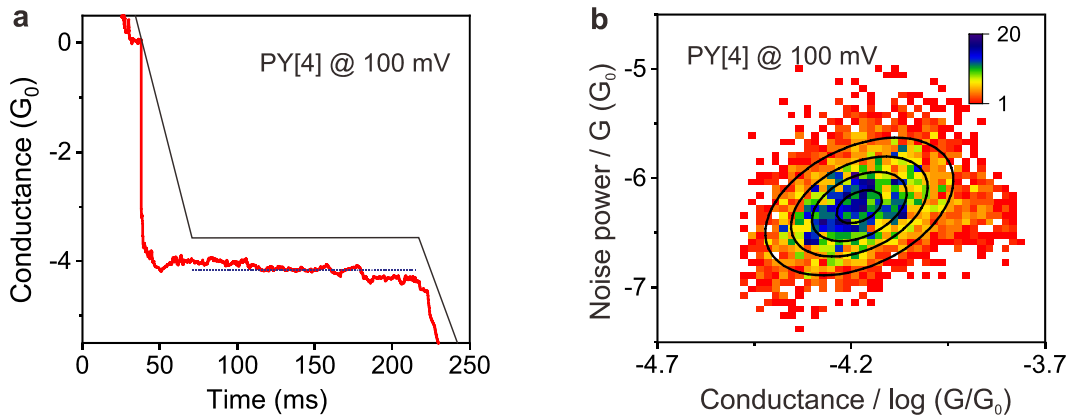


Figure S12. Flicker noise measurements of PY[4] molecular junctions. (a) Representative conductance-displacement traces for the noise measurement at a fixed bias of 100 mV. The piezo for the tip control is paused for 150 ms when a stable molecular junction is formed. The black line indicates the ramp of the piezo voltage, and the dashed blue line indicates the average conductance of the junction (G_{AVG}). (b) The normalized flicker noise power versus average conductance of the junctions at a bias of 100 mV, constructed from 24060 conductance traces.

A discrete Fourier transform of the conductance is performed and squared to get the the noise power spectral density (PSD). To quantify the noise level, PSD is numerically integrated from 100 Hz to 1 kHz for each molecular junction. This value is used as the flicker noise power. Figure 12a shows a typical conductance traces of PY[4] molecular junction at a fixed bias of 100 mV, and Figure 12b displays a 2D histogram of flicker noise power normalized by G_{AVG} against the junction conductance constructed from 24060 conductance traces.

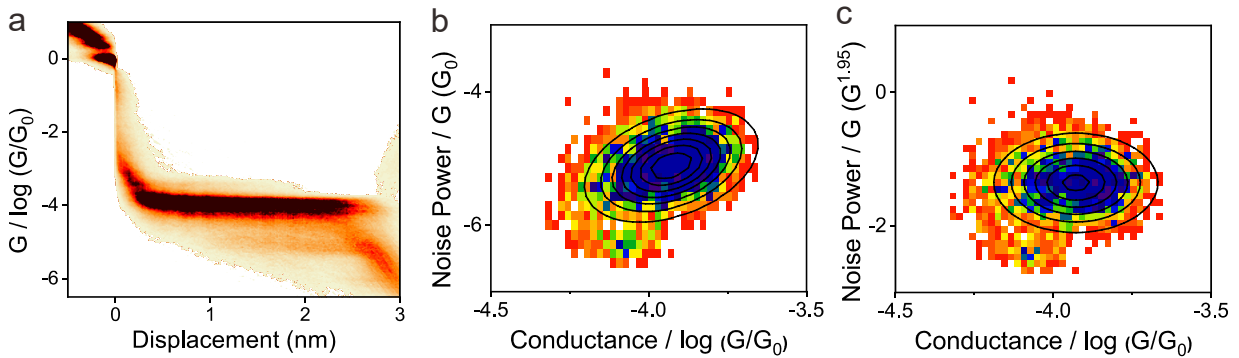


Figure S13. Flicker noise of PY[2] molecular junctions at low conductance state. (a) 2D histogram of conductance-displacement traces for the noise measurement at a fixed bias of 100 mV. The piezo for the tip control is paused for 150 ms when the low conductance state of the PY[2] molecular junction is formed. (b) 2D histogram of normalized flicker noise power against average junction conductance for molecule PY[2]. Dotted contours represent fits to the bivariate normal distribution. (c) 2D histograms of flicker noise power normalized by $G^{1.95}$ against average conductance.

5. DFT calculation of electron transport through molecular junctions

In this study, we employed the software package QuantumATK (version 2020.09), which is based on density functional theory combined with non-equilibrium Green's function, to perform the geometric optimization and calculate the electron transport through the molecular junctions. The molecule is connected to the Au (111)-(4×4) surfaces *via* the nitrogen-gold bond in pyridine-anchored molecular junctions. The Perdew-Burke-Ernzerhof (PBE) functional with generalized gradient approximation is used to describe the electronic exchange and correlation for all atoms. The double- ζ plus polarization (DZP) basis set is adopted for all atoms. The real space grid techniques are used with the energy cutoff of 150 Ry in numerical integrations. The k-point samplings for calculations of electronic transport properties are 4×4×150 in the x, y, and z transport directions, respectively. The criteria of convergence for energy and force were set to be 1×10^{-5} eV and 0.01 eV \AA^{-1} , respectively. The transmission coefficient $T(E, V_{ds})$ at a given bias voltage V_{ds} is calculated by the formula: $T(E, V_{ds}) = \text{Tr}[\Gamma_S(E)G^R(E)\Gamma_D(E)G^A(E)]$, where $G^R(E)$ and $G^A(E)$ are the retarded and advanced Greens functions of the scattering region, respectively.

Figure S14 shows the electron transmission pathways on the LUMO of PY[4] molecular junction with tilt angles of 45° and 0° . By utilizing electron transmission pathways, we were able to split the transmission coefficient into local bond contributions. Our analysis revealed the volumes of the arrows on the nitrogen–gold bonds decrease as the tilt angles change from 45° to 0° , indicating that the strength of the electronic coupling between the gold electrode and the molecular π^* orbital decreases when the nitrogen-gold bonds aligns with the pyridine plane.

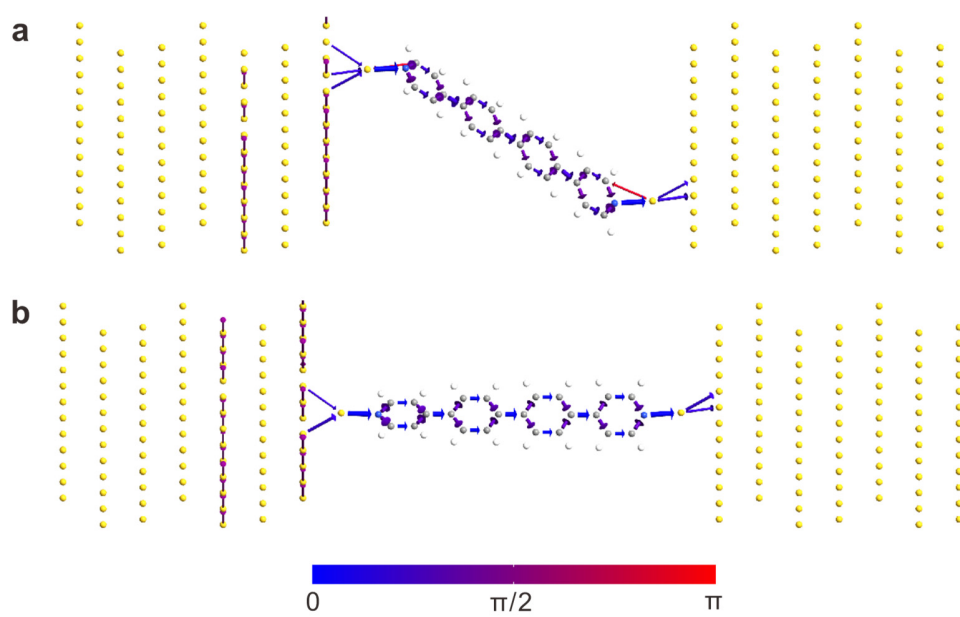


Figure S14. The electron transmission pathways on LUMO of PY[4] molecular junctions under the tilt angle of 45° (a) and 0° (b), respectively. The direction (color) of the arrows indicate the direction of the electron transport. The magnitudes of the pathway are illustrated by the volume of the arrows.

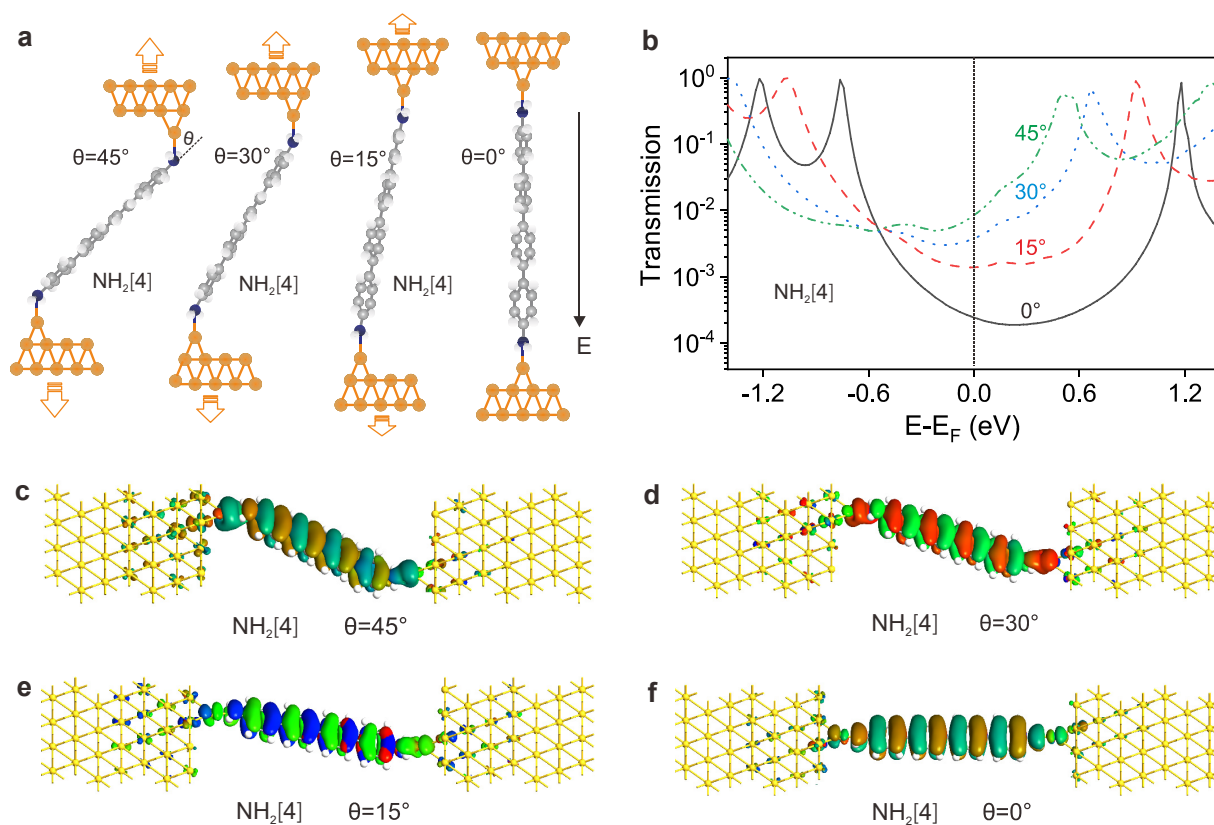


Figure S15. Transmission characteristics of NH₂[4] molecular junction with different tilt angle between the nitrogen-gold bond and the benzene plane. (a) Examples of junction geometries relaxed with different nitrogen nitrogen-gold bond orientations. (b) Transmission characteristics plotted on the semi-logarithmic scale for the molecular junctions. The green dotted, blue dashed, red dashed and black solid lines denote the angle (θ) between nitrogen-gold bond and benzene ring plane is 45° , 30° , 15° and 0° , respectively. The transmission spectrum changes drastically as the tilt angle altered, which indicates that the conductance of NH₂[4] molecular junction will change as the tilt angle changes. However, this deduction is contrast to the experimental observation, and thus we assume that the initial angle (θ) is already 0° for NH₂[4] molecular junction before stretching. (c-f) Spatial distribution of LUMO with a tilt angle of 45° , 30° , 15° , and 0° , respectively.

6. Molecular electrostatic potential distribution.

We use Gaussian software to calculate the electrostatic potential of two different types of molecules. In order to obtain a more accurate molecular surface electrostatic potential map, we firstly optimized the initial molecular structure through the DFT (b3lyp) method 6-31g(d) basis set, obtaining the stable conformation with the lowest energy in the gas or liquid phase. Self-Consistent Field (SFC) was selected as the density matrix to calculate the electrostatic potential.

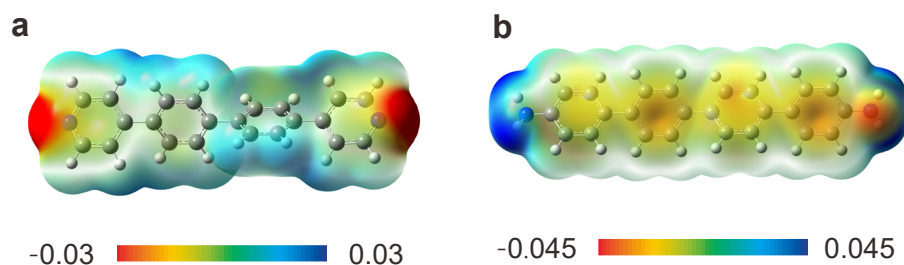


Figure S16. Molecular electrostatic potential distribution. Calculated electrostatic potential mapping for (a) PY[4] and (b) NH₂[4]. The red color represents a negative charge, while the blue color represents a positive charge. ESP unit: Hartree/e.

7. Reference

1. Z. Yu, Y.-X. Xu, J.-Q. Su, P. M. Radjenovic, Y.-H. Wang, J.-F. Zheng, B. Teng, Y. Shao, X.-S. Zhou and J.-F. Li, Probing Interfacial Electronic Effects on Single-Molecule Adsorption Geometry and Electron Transport at Atomically Flat Surfaces, *Angew. Chem. Int. Ed.*, 2021, **60**, 15452-15458.